

ANALYSIS OF SECOND MOMENT CLOSURE MODELING FOR A RECTANGULAR SURFACE JET USING DNS DATA

Iftekhar Z. Naqavi

Department of Mechanical and Materials Engineering
McLaughlin Hall, Queen's University
Kingston, Ontario, Canada K7L 3N6
naqavi@appsci.queensu.ca

Robert J. Martinuzzi

Department of Mechanical and Manufacturing Engineering
Schulich School of Engineering, University of Calgary
2500 University Drive NW, Calgary, Alberta, Canada T2N 1N4
rmartinu@ucalgary.ca

Eric Savory

Department of Mechanical and Materials Engineering
The University of Western Ontario
London, Ontario, Canada N6B 5A9
esavory@eng.uwo.ca

ABSTRACT

Results for a DNS of a horizontal, rectangular turbulent surface jet of aspect ratio 2:1 at a Reynolds number of 4,420 issuing into a quiescent medium are presented. The simulation is validated against experimental data. The DNS results are used to investigate sub-models used in the RANS "Basic Model" and TCL model. It is shown that the pressure-strain correlation and dissipation anisotropy models incompletely describe the near surface behaviour. These deficiencies negatively impact the prediction of the jet spreading rate and the existence of the surface layer associated with fast variations of the horizontal vorticity component.

INTRODUCTION

Turbulent surface jets are jets that issue close to or at the free surface of large bodies of water for which the turbulent free-surface interaction plays a dominant role in determining the jet structure development. These flows are of significant interest in environmental applications, for example dispersion of pollutants or thermal discharges or oxygenation of micro-flora. Experiments show that the lateral surface spread rate is significantly greater than the vertical (surface normal) spread rate (Anthony and Willmarth, 1992). Moreover, the surface normal velocity and its fluctuations diminish while the lateral and stream-wise velocity fluctuations increase as the surface is approached (Anthony and Willmarth, 1992; Gholamreza-Kashi et al., 2007). This behaviour is related to surface-vorticity interactions occurring in a very thin layer close to the surface, which has been difficult to resolve

experimentally. A strong motivation thus exists to use numerical simulations to gain further insight.

Reynolds Averaged Navier-Stokes (RANS) simulations of the turbulent surface jet have proven challenging. For example, simulations with a second-moment closure using the 'Basic Model' over-predicted the lateral jet spread rate by a factor of 5, under-predicted the vertical jet spread rate and under-predicted the mean-stream wise velocity (Craft et al., 2000). Another model, known as TCL (Two Component Limit), gives some improvement but the spread rates are still over-predicted. Moreover, the velocity decay rates for the TCL are higher than the experimental values.

Large eddy simulation (LES) or direct numerical simulation (DNS) might offer a useful simulation approach. Mangiavacchi et al. (1994) performed a temporal DNS of a circular surface jet issuing one diameter below the surface. The DNS showed the existence and development of the coherent structures in this jet but no statistics were generated. Shen et al. (1999) used DNS to examine the free-surface turbulence over a two-dimensional mean shear flow. They conceptually identified the surface layer (a thin region adjacent to the free surface) characterized by the fast variation of the horizontal vorticity components. Based on these observations, it might be expected that the surface-layer plays an important role in the local behaviour of the pressure-rate-of-strain and dissipation rate tensors. Improving the RANS predictions of surface flows thus appears related to a better modeling of the non-dispersive pressure correlation terms, the dissipation rate transport equation and the dissipation rate anisotropy, especially close to the surface.

In this work, the different closure models used in the TCL and "Basic Model" are analyzed using the data from a DNS

of a horizontal, rectangular, turbulent surface jet at a Reynolds number of 4,420. For this purpose, the flow field from DNS is used to calculate the values of the pressure correlation term and dissipation rate directly. It is shown that even for the case of the best possible dissipation rate estimates, the pressure correlation and dissipation anisotropy models require closer attention in the near surface region.

SIMULATION DETAILS AND VALIDATION

In this work the DNS is performed with an in-house code. In this section, a brief overview of the methodology is provided and particular attention is given to the validation of the simulation results.

The momentum equations are solved using a fractional step scheme with a collocated arrangement of variables (Zang et al., 1994). The spatial derivatives are discretized with a second-order central difference scheme. The solution is advanced in time with a semi-implicit scheme. The resulting system of equations is solved using a parallel the BiCGstab solver.

A schematic representation of the physical domain for the rectangular surface jet, width-to-depth ratio of $b/h = 2$, with some relevant quantities, is shown in Fig. 1. The x , y and z -axis are in the stream-wise, lateral span-wise and normal to the surface directions respectively. The jet exit is located at the plane $x = 0$. Here, u , v and w are the instantaneous stream-wise, lateral span-wise and surface normal velocities respectively, for which U, V, W are the mean and u', v', w' are the fluctuating components. The maximum stream-wise velocity U_{max} in the developed region of the jet occurs at the free surface at the jet plane of symmetry. The jet half depth L_z is the vertical distance from the surface and the jet half width L_{ys} is the lateral distance from the jet plane of symmetry where $U = U_{max}/2$. The jet half width L_y is the lateral distance from the jet plane of symmetry at the depth of L_z where $U = U_{max}/4$.

The DNS of the surface jet is validated through the grid independence test and comparison with the experimental data. Three different grids 'Grid 1', 'Grid 2' and 'Grid 3' with 3.5, 5.5 and 8.5 million grid points are used. The vertical profiles of mean stream-wise velocity U are shown at $x = 16D$ along the jet plane of symmetry for the three grids in Fig. 2(a), where D is the hydraulic diameter of the initial jet. Figure 2(b) shows the vertical profiles of the turbulence kinetic energy (TKE) ' k^2 ' at $x = 16D$ along the jet plane of symmetry for the three grids. Although the differences between the grids are slightly larger than for the mean stream-wise velocity profiles, convergence towards the finest grid is clear. This convergence, with increasing grid resolution, shows that the numerical error in the simulation is well-behaved and decreasing as expected, whilst all the grids give the same profile shapes. It was also verified that the grid size was of the same order as the local dissipation scale.

The simulation results are also compared with the experimental data of Gholamreza-Kashi et al. (2007) for a

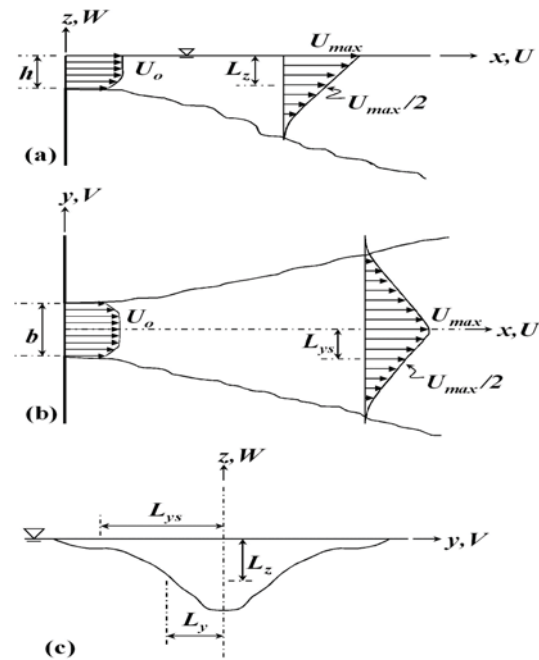


Fig. 1. The physical domain and nomenclature for a rectangular surface jet, (a) jet plane of symmetry, (b) plan view and (c) cross-sectional view.

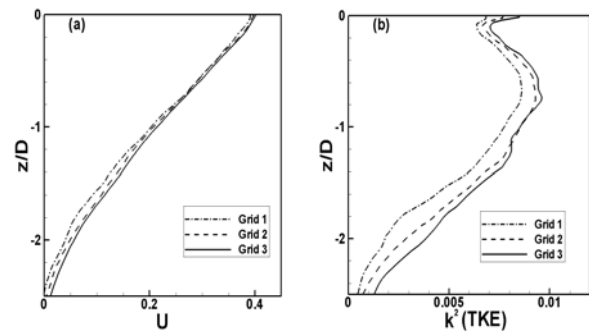


Fig. 2. Grid independence test for three different grids (a) mean stream-wise velocity profile (b) turbulence kinetic energy, at the jet plane of symmetry at $x = 16D$.

rectangular surface jet at the same Reynolds number (Re_b) of 4,420. The vertical profiles of mean stream-wise velocity at the plane of symmetry of the jet are compared with the experimental data (open symbols) in Fig. 3. The velocity profiles in Fig. 3(a) at $x = 2D, 4D, 6D$ and $8D$ represent the transition region of the jet and Fig. 3(b) shows the velocity profiles at $x = 12D, 16D$ and $20D$ in the developed region of the jet. The velocity profiles in the developed region asymptotically approach self-similar behaviour and match the experimental data within the experimental uncertainty. The root mean square (rms) velocities along the surface normal direction at the jet plane of symmetry are shown in Fig. 4. The comparison of jet spread rate in the vertical direction, L_z , at the jet plane of symmetry and in the horizontal direction at the surface, L_{ys} , normalized by the

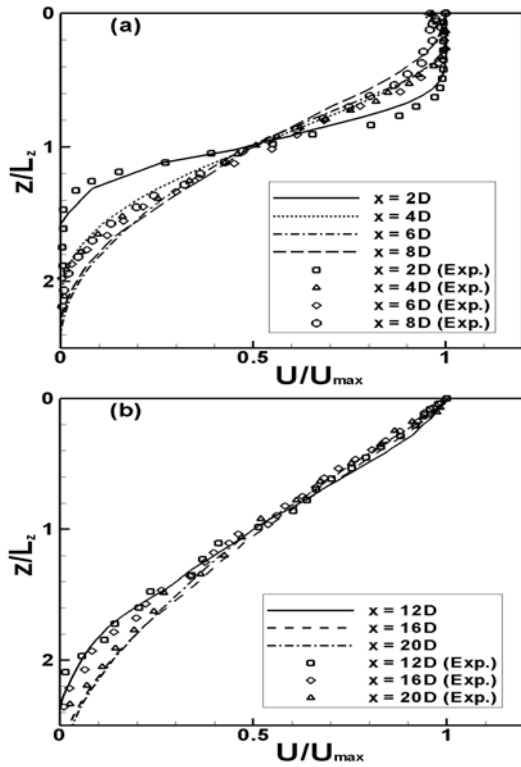


Fig. 3. Mean stream-wise velocity profiles along the jet plane of symmetry (a) the transition region, (b) the fully developed region ((Exp) Gholamreza-kashi et al. (2007)).

jet inlet depth h , are shown in Fig. 5 as a function of the normalized stream-wise distance x/D . The DNS results are in good agreement with the experimental data and show that the simulation gives physically realizable results for a rectangular surface jet.

RESULTS AND DISCUSSIONS

RANS with second moment closure models has been used to study the surface jet (cf. Craft et al., 2000). The results show that the second moment closure is not able to predict the main parameters such as jet spread rate, mean and rms velocities satisfactorily. The Reynolds stress $\langle u'_i u'_j \rangle$ transport equation for second-moment modeling is given as:

$$\frac{D \langle u'_i u'_j \rangle}{Dt} = \Pi_{ij} + P_{ij} + d_{ij} - \varepsilon_{ij} \tag{1}$$

where: $\Pi_{ij} = -\langle u'_i u'_k \rangle \partial U_j / \partial x_k - \langle u'_i u'_k \rangle \partial U_i / \partial x_k$ is the generation due to the strain field; $P_{ij} = \langle p' (\partial u'_i / \partial x_j + \partial u'_j / \partial x_i) \rangle$ is the non-dispersive pressure correlation or pressure-rate-of-strain tensor; d_{ij} is diffusivity ε_{ij} and is the dissipation rate tensor. Except for the generation term, which is exact, P_{ij} , d_{ij} and ε_{ij} need to be modeled. The diffusivity term is usually modeled with an eddy-viscosity based scheme. However, the non-dispersive pressure correlation term and dissipation rate tensor are modeled with more sophisticated schemes.

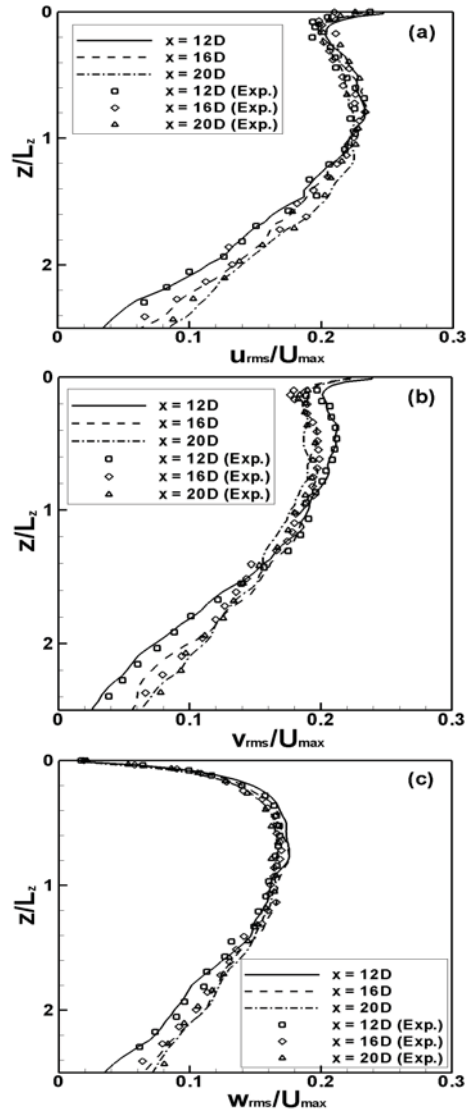


Fig. 4. The vertical profiles of rms velocity in the developed region at the jet plane of symmetry (a) u_{rms} , (b) v_{rms} and (c) w_{rms} ((Exp) Gholamreza-kashi et al. (2007)).

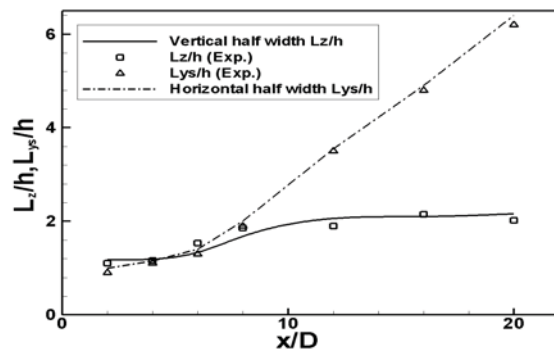


Fig. 5. The jet spread rate in the horizontal direction at the surface and in the vertical direction at the jet plane of symmetry ((Exp) Gholamreza-kashi et al. (2007)).

The non-dispersive pressure correlation terms are modeled with the 'Basic Model' (BM) and 'Two Component Limit' or TCL model (Craft et al., 2000) as given in appendix eq. (1A) and (2A), respectively. The DNS data are

used to examine the behaviour of these models. The exact values of the pressure-rate-of-strain tensor P_{ij} from the DNS data (lines), along with its model values for the 'Basic Model' (closed symbols) and TCL (open symbols), are given in Fig. 6 at $x = 12D$ along the jet plane of symmetry. Broglio et al. (2003) suggested that the P_{ij} distributes the energy among the normal Reynolds stresses $\langle u'u' \rangle$, $\langle v'v' \rangle$ and $\langle w'w' \rangle$. The stream-wise normal stress $\langle u'u' \rangle$ extract the energy from the mean shear field and P_{11} transfers the energy to the other two components. They describe the general behaviour of the pressure-rate-of-strain tensor for a free surface: P_{11} is negative over most of the flow domain except very close to the surface; P_{22} remains positive throughout the domain and P_{33} is positive away from the surface, but becomes negative on approaching the surface. The diagonal components of P_{ij} shown in Fig. 6(a) for the current DNS show a similar behaviour, which is characteristic of that reported for other free surface flows literature.

The RANS model predictions, however, show some important differences. The span-wise component P_{22} is reasonably predicted by the TCL model, but the Basic Model yields a significant over-prediction. The surface normal component P_{33} is very important for free surface flows, particularly very close to the surface. The TCL model predictions for this component are close to those of the DNS in the bulk of the jet, but fail to change sign near the free surface. The Basic model predicts only negative values for P_{33} and very close to the surface, where the DNS data change sign from positive to negative, it over predicts by a factor of 2.

Defects in the prediction of the pressure-rate-of-strain tensor have direct consequences for the jet spread rates. Generally, negative values for any diagonal component of P_{ij} imply a transfer of energy from the corresponding Reynolds normal stress to other components and conversely for a positive value. The DNS data show that in the bulk of the jet, P_{11} is negative, while P_{22} and P_{33} are positive: energy is transferred from $\langle u'u' \rangle$ to both $\langle v'v' \rangle$ and $\langle w'w' \rangle$. Near the free surface P_{33} becomes negative and P_{11} becomes positive, however in the region where P_{33} becomes negative $|P_{11}| < |P_{22}|$ and most of the energy from $\langle w'w' \rangle$ transfers to $\langle v'v' \rangle$.

The Basic model under-predicts negative P_{11} , whilst P_{33} is also negative from the bulk of the jet to the free surface with a very large negative value near the surface. The Basic model contributes a large amount of energy to $\langle v'v' \rangle$ from the other two components, especially near the free surface. The large lateral fluctuations near the surface result in an over-prediction of the horizontal spread rate of the jet along the surface. The negative P_{33} in the bulk of the jet also

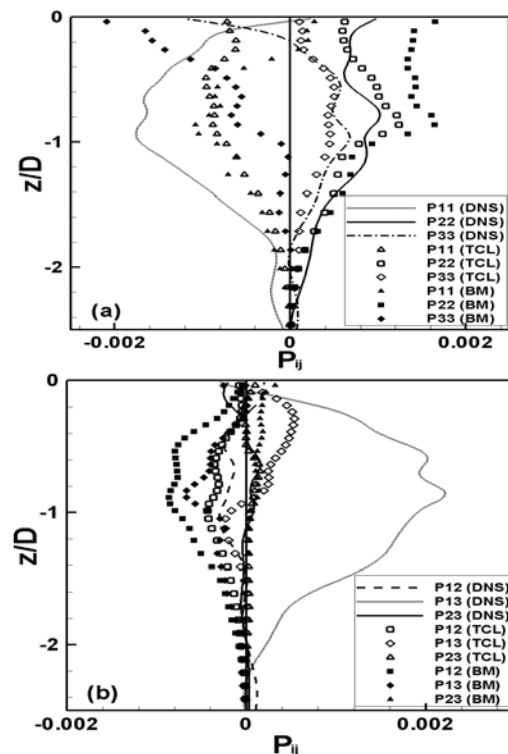


Fig. 6. Comparison of pressure rate of strain tensor terms for DNS, the Basic Model and TCL model along the jet plane of symmetry at $x=12D$ (a) the diagonal and (b) the off-diagonal terms.

means that there is no transfer of energy to vertical fluctuations due to pressure-rate-of-strain and the overall contribution to $\langle w'w' \rangle$ will be lower, which results in an under-prediction of the jet vertical spread rate.

The TCL model gives positive P_{22} and P_{33} , while P_{11} is negative which results in energy transfer from $\langle u'u' \rangle$ to the other two components. The $\langle v'v' \rangle$ component gets the larger share of this energy transfer because $|P_{33}| < |P_{22}|$ near the surface. Moreover, $\langle u'u' \rangle$ has larger energy content near the surface and can transfer much more energy to other components than $\langle w'w' \rangle$. Consequently, the lateral spread rate is over-predicted. The surface normal component P_{33} is also positive, resulting in some energy transfer to $\langle w'w' \rangle$. Near the surface, vertical fluctuations go to zero because of the boundary, but due to the non-local character of pressure the effect of energy transfer to $\langle w'w' \rangle$ can appear away from the surface as an over-predicted vertical jet spread rate.

The off-diagonal terms of pressure-rate-of-strain tensor are shown in Fig. 6(b). The DNS data show that P_{12} and P_{23} are much smaller than P_{13} . The Basic model does not capture the behaviour observed in the DNS. The TCL model severely under predicts P_{13} . The contribution of off-diagonal terms is complicated, P_{13} interacts with $\langle u'u' \rangle$ via

$\Pi_{11} = -\langle u'u' \rangle \partial U / \partial x + \langle u'v' \rangle \partial U / \partial y + \langle u'w' \rangle \partial U / \partial z$. With $\langle u'w' \rangle < 0$, P_{13} contributes positively to $\langle u'u' \rangle$. However, the under predicted TCL-values result in less contribution to $\langle u'u' \rangle$ and a higher velocity stream-wise decay rate.

The dissipation rate tensor is also modeled for second moment closures. The TCL model, given in equation (A3), is designed to give anisotropic estimates for the dissipation tensor. The total dissipation is modeled through equation (A4). The DNS data are used to verify the behaviour of the total dissipation model equation. The terms involved in equation (A4) are presented in Fig. 7 for $x = 12D$ at the jet plane of symmetry. The terms involved in equation (A4) are: T1 (Convection term); T2 (Strain term); T3 (Sink term) and T4 (Diffusion term). Figure 7 suggests that diffusion term is almost an order of magnitude larger than the other terms in the bulk of the jet and near the surface it is almost two orders of magnitude greater. The residual of equation (A4), based on the DNS data, is almost of the same order as the dissipation term in most of the domain and near the surface it becomes two orders of magnitude larger. Hence, the total dissipation model does not satisfy the DNS data.

The dissipation rate tensor given by the equation (A3) is also calculated using the DNS data. The TCL-modeled values of the dissipation rate tensor and the DNS values are compared in Fig. 8 at $x = 12D$ along the jet plane of symmetry. The raw values of the dissipation rate tensor suggest that the model gives anisotropic values for the three components \mathcal{E}_{11} , \mathcal{E}_{22} and \mathcal{E}_{33} , particularly near the free surface. However, comparison with the DNS data shows that the model over-predicts these values. Moreover, near the free surface, the model is unable to reproduce the behaviour observed in the DNS data. The dissipation rate tensor values are scaled with total dissipation rate in Fig. 8(b) to show that the relative level of anisotropy given by the model is significantly less than seen in the DNS data. Upon closer examination of equation (A3), all the terms in the model of the dissipation strain tensor are scaled with the Reynolds stresses. Figure 4 shows that the Reynolds stresses near the surface are anisotropic. While it can be inferred that near the surface, scaling with the Reynolds stresses might result in anisotropic values for the dissipation rate tensor, the DNS results suggest that this form for the scaling is incomplete.

CONCLUSIONS

Two second moment closure models for RANS simulations of free surface flows are examined using DNS data to evaluate the pressure-rate-of-strain tensor model and dissipation rate tensor model at the jet plane of symmetry. The TCL model appears to give better estimates than the “Basic Model” away from the surface. However, near the surface, both models show important deficiencies when compared to the DNS simulation results. The dissipation rate tensor model shows anisotropic behaviour near the surface, but over-predicts the dissipation rate tensor. The near surface behaviour of the dissipation rate tensor given by the DNS data is due to the presence of the surface layer (Shen et al., 1999), which is a thin region below the free

surface where surface normal gradients change rapidly and surface normal vorticity generates. RANS models do not account for this surface layer.

REFERENCES

Anthony, D.G. and Willmarth, W.W., 1992, “Turbulence measurements in a round jet beneath a free surface”, *J. Fluid Mech.*, Vol. 243, pp. 699-720.
 Broglia, R., Pascarelli, A. and Piomelli, U., 2003, “Large-eddy simulation of ducts with a free surface”, *J. Fluid Mech.*, Vol. 484, pp. 223-253.
 Craft, T. J., Kidger, J. W., Launder, B. E., 2000, “Second-moment modeling of developing and self-similar 3D turbulent free-surface jets”, *Int. J. Heat and Fluid Flow*, Vol. 21, pp. 338-344.
 Gholamreza-Kashi, S., Martinuzzi, R. J. and Baddour, R. E., 2007, “Mean flow field of a nonbuoyant rectangular surface jet”, *ASCE J. Hydraul. Eng.*, Vol. 133(2), pp. 234-239.
 Mangiavacchi, N., Gundlapalli, R. and Akhavan, R., 1994, “Dynamics of a turbulent jet interacting with a free surface”, *Free-surface turbulence; Proceedings of the Symposium, 1994 ASME FED Summer Meeting*, Lake Tahoe, NV; United States.
 Shen, L., Zhang, X., Yue, D. K. P. and Triantafyllou, G., 1999, “The surface layer for free-surface turbulent flows”, *J. Fluid Mech.*, Vol. 386, pp. 167-212.
 Zang, Y., Street, R.L. and Koseff, J.R., 1994, “A non-staggered grid, fractional step method for time-dependent incompressible Navier-Stokes equations in curvilinear coordinates”, *J. Comput. Phys.*, Vol. 114, pp. 18-33.

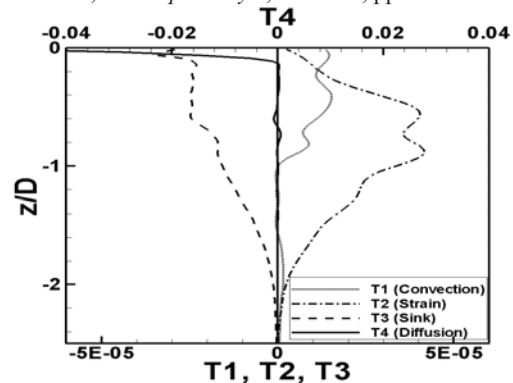


Fig. 7. Vertical profiles of different terms involved in the dissipation model of equation (A4).

APPENDICES

The Basic Model for the pressure-rate-of-strain tensor is give as:

$$P_{ij} = -c_1 \epsilon a_{ij} - c_2 \left(\Pi_{ij} - \frac{1}{3} \Pi_{kk} \delta_{ij} \right) + P_{ij}^{wr} \quad (A1)$$

where

$$P_{ij}^{wr} = \text{wall reflection term}$$

$$a_{ij} = \langle u'_i u'_j \rangle / k - \frac{2}{3} \delta_{ij} \quad c_1 = 1.8 \quad c_2 = 0.6$$

The TCL model is given as:

$$\begin{aligned}
 P_{ij} = & -c_1 \varepsilon \left[a_{ij} + c'_1 \left(a_{ik} a_{kj} - \frac{1}{3} A_2 \delta_{ij} \right) \right] \\
 & - \varepsilon A^{1/2} a_{ij} - 0.6 \left(\Pi_{ij} - \frac{1}{3} \delta_{ij} \Pi_{kk} \right) + 0.3 a_{ij} \Pi_{kk} \\
 & - 0.2 \left[\frac{\langle u'_k u'_j \rangle \langle u'_l u'_i \rangle}{k} \left[\frac{\partial U_k}{\partial x_l} + \frac{\partial U_l}{\partial x_k} \right] \right. \\
 & \left. - \frac{\langle u'_l u'_k \rangle}{k} \left[\langle u'_i u'_k \rangle \frac{\partial U_j}{\partial x_l} + \langle u'_j u'_k \rangle \frac{\partial U_i}{\partial x_l} \right] \right] \\
 & - c_2 \left[A_2 \left(\Pi_{ij} - D_{ij} \right) + 3 a_{mi} a_{nj} \left(\Pi_{mn} - D_{mn} \right) \right] \\
 & + c'_2 \left\{ \left(\frac{7}{15} - \frac{A_2}{4} \right) \left(\Pi_{ij} - \frac{1}{3} \delta_{ij} \Pi_{kk} \right) \right. \\
 & \left. + 0.1 \left[a_{ij} - \frac{1}{2} \left(a_{ik} a_{kj} - \frac{1}{2} \delta_{ij} A_2 \right) \right] \Pi_{kk} \right. \\
 & \left. - 0.05 a_{ij} a_{lk} \Pi_{kl} \right. \\
 & \left. + 0.1 \left[\left(\frac{\langle u'_i u'_m \rangle}{k} \Pi_{mj} + \frac{\langle u'_j u'_m \rangle}{k} \Pi_{mi} \right) \right. \right. \\
 & \left. \left. - \frac{2}{3} \delta_{ij} \frac{\langle u'_l u'_m \rangle}{k} \Pi_{ml} \right] \right. \\
 & \left. + 0.1 \left[\frac{\langle u'_i u'_i \rangle \langle u'_k u'_j \rangle}{k^2} - \frac{1}{3} \delta_{ij} \frac{\langle u'_l u'_m \rangle \langle u'_k u'_m \rangle}{k^2} \right] \right. \quad (A2) \\
 & \times \left[6 D_{lk} + 13 k \left[\frac{\partial U_l}{\partial x_k} + \frac{\partial U_k}{\partial x_l} \right] \right] \\
 & \left. + 0.2 \frac{\langle u'_l u'_i \rangle \langle u'_k u'_j \rangle}{k^2} \left(D_{lk} - \Pi_{lk} \right) \right\}
 \end{aligned}$$

where

$$D_{ij} = - \left(\langle u'_i u'_k \rangle \frac{\partial U_k}{\partial x_j} + \langle u'_j u'_l \rangle \frac{\partial U_l}{\partial x_i} \right)$$

The dissipation equation is given as:

$$\frac{D\varepsilon}{\underbrace{Dt}_{T_1}} = c_{\varepsilon 1} \underbrace{\frac{\varepsilon \Pi_{kk}}{2k}}_{T_2} - c_{\varepsilon 2} \underbrace{\frac{\varepsilon^2}{k}}_{T_3} + \underbrace{d_{\varepsilon}}_{T_4} \quad (A3)$$

where,

$$d_{\varepsilon} = \frac{\partial}{\partial x_k} \left[\left(\nu + \frac{\nu_t}{\sigma_{\varepsilon}} \right) \frac{\partial \varepsilon}{\partial x_k} \right]$$

The dissipation strain tensor is given as:

$$\varepsilon_{ij} = (1 - A) (\varepsilon'_{ij} + \varepsilon''_{ij}) / D + \frac{2}{3} A \varepsilon \delta_{ij} \quad (A4)$$

with,

$$\varepsilon'_{ij} = \varepsilon \frac{\langle u'_i u'_j \rangle}{k} + 2\nu \frac{\langle u'_i u'_n \rangle}{k} \frac{\partial \sqrt{k}}{\partial x_i} \frac{\partial \sqrt{k}}{\partial x_n} \delta_{ij}$$

$$+ 2\nu \frac{\langle u'_l u'_i \rangle}{k} \frac{\partial \sqrt{k}}{\partial x_j} \frac{\partial \sqrt{k}}{\partial x_l} + 2\nu \frac{\langle u'_l u'_j \rangle}{k} \frac{\partial \sqrt{k}}{\partial x_i} \frac{\partial \sqrt{k}}{\partial x_l}$$

$$\varepsilon''_{ij} = \varepsilon (1 - A) \left[2 \frac{\langle u'_l u'_k \rangle}{k} d_l^A d_k^A \delta_{ij} \right.$$

$$\left. - \frac{\langle u'_i u'_i \rangle}{k} d_l^A d_j^A - \frac{\langle u'_l u'_j \rangle}{k} d_l^A d_i^A \right]$$

$$D = (\varepsilon'_{kk} + \varepsilon''_{kk}) / (2\varepsilon)$$

$$N_i = \partial (k^{3/2} A^{1/2} / \varepsilon) / \partial x_i$$

$$d_i^A = N_i / (0.5 + (N_k N_k)^{1/2})$$

For model coefficients and constants see Craft et al. (2000).

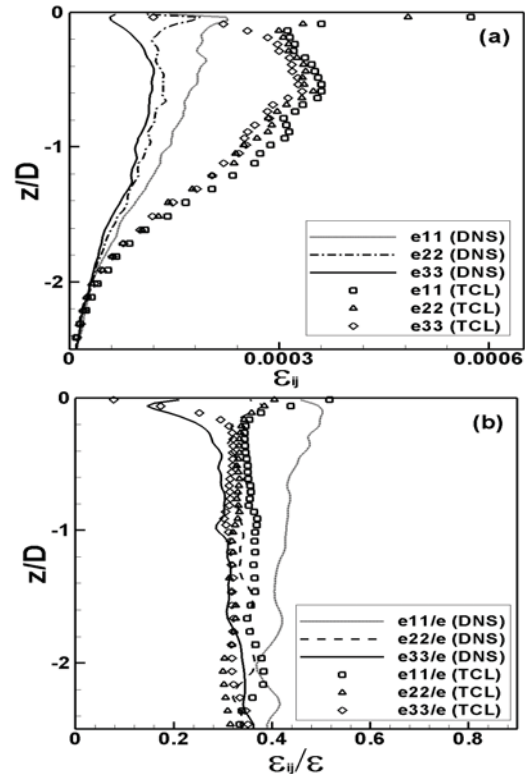


Fig. 8. Comparison of the diagonal terms of the dissipation rate tensor from TCL model (A3) with the DNS data (a) raw values of ε_{ij} and (b) scaling with total dissipation ε to show the level of anisotropy.